nature photonics

LETTERS

https://doi.org/10.1038/s41566-019-0577-1

Efficient near-infrared light-emitting diodes based on quantum dots in layered perovskite

Liang Gao[1,2,9], Li Na Quan[1,9], F. Pelayo García de Arquer[1,9], Yongbiao Zhao[3], Rahim Munir[4,5], Andrew Proppe[1,6], Rafael Quintero-Bermudez[1], Chengqin Zou[1], Zhenyu Yang[1], Makhsud I. Saidaminov[1], Oleksandr Voznyy[1], Sachin Kinge[7], Zhenghong Lu[3], Shana O. Kelley[6,8], Aram Amassian[4], Jiang Tang[2*] and Edward H. Sargent[1*]

Light-emitting diodes (LEDs) based on excitonic material systems, in which tightly bound photoexcited electron–hole pairs migrate together rather than as individual charge carriers, offer an attractive route to developing solution-processed, high-performance light emitters. Here, we demonstrate bright, efficient, excitonic infrared LEDs through the incorporation of quantum dots (QDs)[1] into a low-dimensional perovskite matrix. We program the surface of the QDs to trigger fast perovskite nucleation to achieve homogeneous incorporation of QDs into the matrix without detrimental QD aggregation, as verified by in situ grazing incidence wide-angle X-ray spectroscopy. We tailor the distribution of the perovskites to drive balanced ultrafast excitonic energy transfer to the QDs. The resulting LEDs operate in the short-wavelength infrared region, an important regime for imaging and sensing applications, and exhibit a high external quantum efficiency of 8.1% at 980 nm at a radiance of up to 7.4 W Sr^{-1} m^{-2}.

Efficient infrared sources are of interest for night vision[1] and optical communications[2] as well as biological and medical applications[3]. The development of infrared sources that combine high brightness and high efficiency is challenging. Present-day infrared technologies rely on costly high-temperature epitaxial semiconductors[4–6], which limits integration with other material systems, such as Si-based technologies. Solution-processed materials such as organics[7] and perovskites[8–10] have shown promise in the visible light emission that is compatible with Si electronics, but have so far lacked tunability in the infrared. Quantum dots (QDs) exhibit a wide infrared tunability and have been explored as light-emitting diode (LED) active materials[11]. So far, much-needed surface passivation has been achieved using core–shell structures, yet these hamper efficient and balanced charge transport—a crucial prerequisite for bright and efficient light sources.

Recently, the incorporation of QDs into bulk hybrid organic–inorganic perovskites (QDiP)[12] enabled decoupling of charge transport and light emission/sensitization, leading to more efficient optoelectronic devices[13–15]. This system takes advantage of the compelling charge transport properties of metal halide perovskites and the bandgap tunability of infrared PbS QDs.

In QDiP systems, the rapid and imbalanced carrier dynamics in metal halide perovskites[16] leads to asymmetric charge accumulation, high injection currents and thus high Auger recombination. Moreover, at the high QD loadings needed for high-brightness operation at moderate currents, substantial phase segregation occurs, leading to poor passivation and inefficient energy transfer pathways.

A strategy that achieves balanced charge injection into the QDs—thus avoiding charge accumulation—is needed to suppress deleterious non-radiative recombination (such as Auger recombination), thereby enabling high radiative efficiencies be sustained at high injection levels. Avoiding QD aggregation and attaining homogeneous distribution of QDs within the perovskite matrix is also critical to ensure balanced energy transfer[1]. This is especially important at the high QD loadings required for high-brightness LED applications. Finally, stable operation needs to be ensured beyond the characteristic lifetime of solution-processed perovskites[17].

We took the view that to achieve efficient and stable QDiP light-emitting materials it would be important to (1) control the kinetics of perovskite film formation to accommodate evenly dispersed and unaggregated QDs; (2) retain the heteroepitaxial character of the perovskite/QD interface to ensure good QD passivation; and (3) design a perovskite host material that maximizes directed ultrafast energy transfer into the QDs, avoiding imbalanced free carrier accumulation that would promote Auger recombination (Fig. 1a).

Here, we report a QDiP material that, by providing a matrix for QDs composed of reduced-dimensional perovskites, addresses these goals. Only by programming the surface chemistry of QDs with an appropriate perovskite cation to trigger fast perovskite nucleation were we able to achieve a homogeneous dispersion of QDs in the perovskite matrix. In situ grazing incidence wide-angle X-ray spectroscopy (GIWAXS) revealed that QD-in-layered-perovskite (QDLP) samples exhibit faster growth of the tetragonal phase of the host $CsPbBr_3$ layered perovskites. This results in highly ordered QDs that, even at high concentration, show excellent passivation, attributable to their epitaxial incorporation into the perovskite host. Indeed, the QDs fully retain their initial photoluminescence quantum yield (PLQY) of 45% from the solution phase.

[1]Department of Electrical and Computer Engineering, University of Toronto, Toronto, Ontario, Canada. [2]Wuhan National Laboratory for Optoelectronics, Huazhong University of Science and Technology, Wuhan, China. [3]Department of Materials Science and Engineering, University of Toronto, Toronto, Ontario, Canada. [4]KAUST Solar Center (KSC), and Physical Sciences and Engineering Division, King Abdullah University of Science and Technology (KAUST), Thuwal, Saudi Arabia. [5]Helmholtz-Zentrum Berlin für Materialien und Energie, Berlin, Germany. [6]Department of Chemistry, University of Toronto, Toronto, Ontario, Canada. [7]Advanced Technology Materials & Research, Research & Development, Toyota Motor Europe, Toyota Technical Centre, Zaventem, Belgium. [8]Department of Pharmaceutical Sciences, Leslie Dan Faculty of Pharmacy, University of Toronto, Toronto, Ontario, Canada. [9]These authors contributed equally: Liang Gao, Li Na Quan, F. Pelayo García de Arquer. *e-mail: jtang@mail.hust.edu.cn; ted.sargent@utoronto.ca

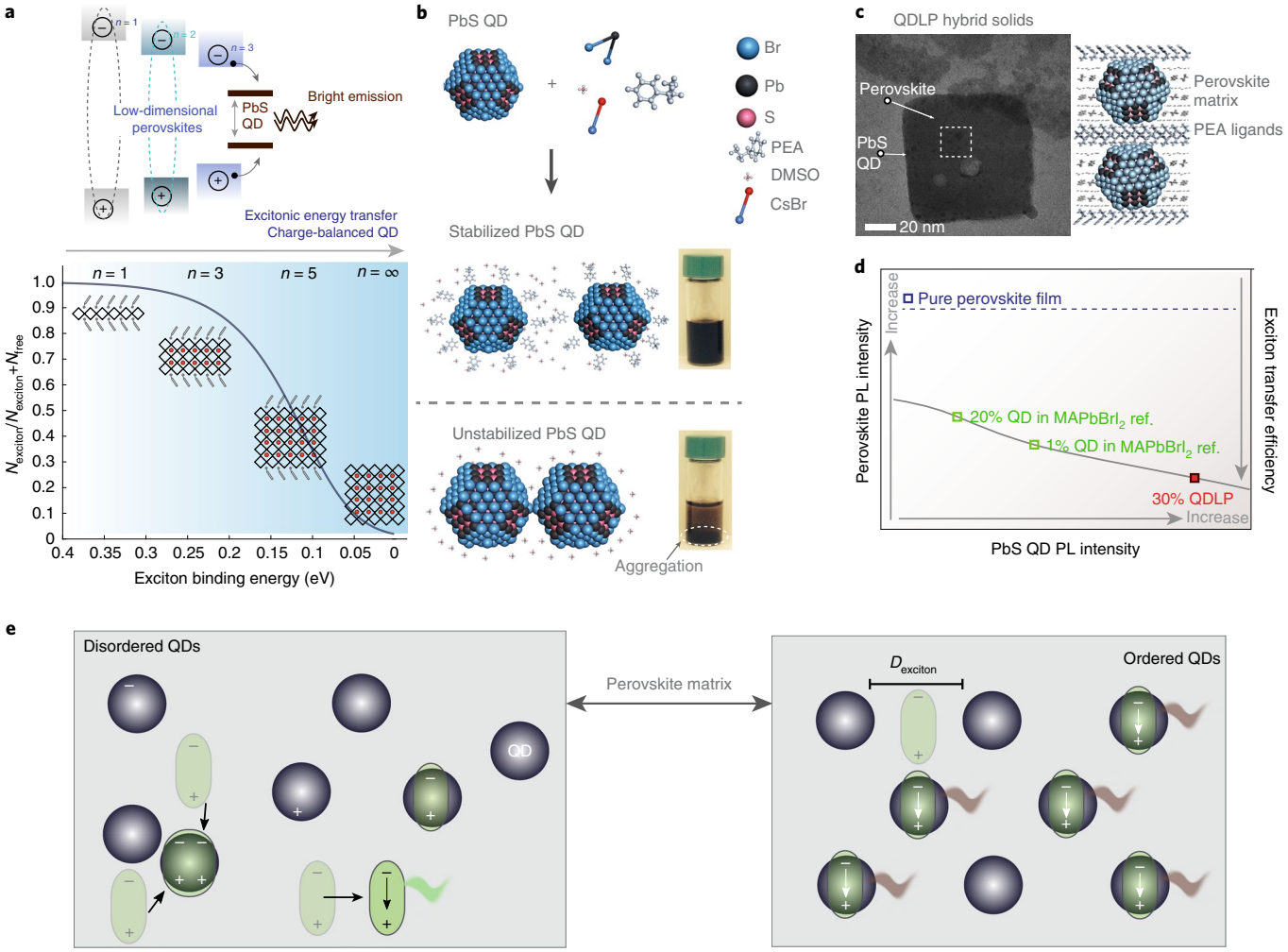

Fig. 1 | QDLP solids and their energy and material properties. a, In QDLP solids, low-dimensional perovskites ($n < 4$) exhibit a strong binding energy and thus a dominant excitonic character. Excitons are transferred from low to high n value perovskites and subsequently into the QDs, where they recombine radiatively. **b**, The components needed to colloidally stabilize the QDs in solution and induce perovskite formation from the QD surface. **c**, High-resolution transmission electron microscopy (TEM) images of PbS QD/perovskite hybrids, directly showing the incorporation of QDs within the perovskite matrix. **d**, Photoexcited energy transfer between PbS QDs and perovskite. The relative PL intensity from the perovskite and QDs indicates efficient incorporation of QDs and also reveals energy transfer from perovskites to QDs. The excitation wavelength is 420 nm. The QD concentration in the QDLP film is defined as the mass ratio of PbS to lead halide. **e**, In a non-homogeneous QDLP solid, energy transfer from the perovskite matrix into the QDs is not efficient, leading to radiative recombination within the perovskite and imbalanced exciton/charge accumulation in the QDs. Energy transfer is optimum when the QDs are homogeneously distributed within one perovskite exciton diffusion length.

We then manipulated the energy landscape of the low-dimensional perovskite host to achieve directed excitonic energy transfer to the QDs, with a transfer efficiency exceeding 80%. This minimizes the unwanted charge accumulation that otherwise promotes non-radiative recombination. We implemented this material in LEDs that are highly emissive at wavelengths across the short-wavelength infrared (SWIR) range, achieving a high external quantum efficiency (EQE) of 8.1% at 980 nm that is sustained even at high radiances up to 7.4 $W\,Sr^{-1}\,m^{-2}$ (a 40-fold improvement in the avoidance of efficiency droop compared to previous QD infrared LEDs) as well as extended device stability.

Earlier strategies to incorporate QDs into metal halide perovskites have relied on a sequential two-step process in which the perovskite matrix is grown around PbI_2-capped QD films by soaking it in methylammonium iodide solution. The difficulty in controlling the kinetics of perovskite nucleation, and the resulting QD distribution within the matrix, resulted in a maximum QD concentration of 28% with a low PLQY of ~0.1%[12]. Moreover, the material suffered from the instability of the perovskite host matrix and from imbalanced charge injection into the QDs. Reliance on free carriers in the matrix led to charge imbalances that promoted Auger recombination at high intensities and limited the EQE and brightness of the resulting LEDs[18].

We took the view that multilayered low-dimensional metal halide perovskites[8,9,19] (perovskites confined two-dimensionally (2D) through bulk organic cations) would offer the required route to control energy transfer into QD embodiments. Depending on the number of perovskite repeat units <n>, layered perovskites exhibit a tunable exciton binding energy that allows transitioning from a fully excitonic character ($n = 1, 2$) to systems with mixed exciton/charge populations ($n > 3$). Moreover, they offer improved robustness, stemming from their higher formation energy[8,9,20]. We focus on phenylethylamine (PEA)–$CsPbBr_3$ perovskites in view of their superior stability compared to organic–inorganic perovskites[21].

To incorporate QDs into reduced-dimensional perovskites, we pursued a new surface exchange to render the as-synthesized QDs

soluble in the perovskite precursor solution. We first considered an exchange consisting of phenylethylamine hydrobromide salt (PEA*HBr or [PEAH$^+$]Br$^-$) dissolved in dimethylformamide (DMF) for high QD incorporation (with a mass ratio of [PEAH$^+$]Br$^-$ to QDs of 2:3) as shown in Supplementary Fig. 1. We then mixed the resulting PEAH$^+$ shelled QD solution in DMF with the perovskite precursor solution containing CsBr and $PbBr_2$ in dimethyl sulfoxide (DMSO). Unfortunately, when we used this approach, the QDs aggregated (Supplementary Fig. 2), probably due to detachment of shell ions (PEAH$^+$) by the polar DMSO solvent molecules (solvation).

We therefore instead pursued an exchange that would program the QD surface with a compound having a binding energy comparable to PEAH$^+$ and reduced solvation potential (by DMSO), thus improving the QD solubility within the precursor solution. With these considerations in mind, we turned our attention to phenethylamine (PEA) as a stabilizing agent (Fig. 1b). As an amine, PEA has a strong binding energy with PbS QDs, and as a neutral molecule it is weakly solvated by DMSO molecules. The resulting solution of exchanged PbS QDs and the perovskite precursor solution with PEA was more stable than the solution without PEA (Supplementary Fig. 2). When other amines such as butylamine (BTA) were used, this resulted in BTA protonation to form BTAH$^+$ with its further incorporation into the perovskite (Supplementary Fig. 3) and a low perovskite-to-QD energy transfer efficiency (Supplementary Figs. 4 and 5); we explain this by the higher basicity of BTA ($pK_a \approx 10.7$) than of PEA ($pK_a \approx 10.0$)[22] leading to protonation of BTA (BTA + PEAH$^+$ → BTAH$^+$ + PEA).

Only when we employed PEA as the QD stabilizing agent did we achieve the incorporation of QDs within the layered perovskites. The resulting QDLP film obtained through a one-step antisolvent deposition method exhibits a very low roughness of ~0.8 nm (root mean square) (Supplementary Fig. 6). TEM images of the QDLP samples reveal the presence of QDs within layered perovskite flakes (Fig. 1c). Among the different QD surface chemistries to incorporate QD in perovskite, PEA-stabilized QDs exhibited the best incorporation, with a stronger photoluminescence in the infrared and the highest energy transfer (Fig. 1d). We hypothesized that this stemmed from a more homogeneous incorporation of QDs within the perovskite excitonic matrix (Fig. 1e). Such an arrangement will lead to a higher probability of QDs accepting excitons and electron/hole pairs.

To investigate the role of PEA$^+$ in enabling the uniform incorporation of QDs into the resulting solids and driving perovskite nucleation, we monitored ex situ and in situ GIWAXS as a function of time (Fig. 2a,b). We confirmed that the QDs act as seeds that induce a fast $CsPbBr_3$ growth stemming from their surface, until PEA$^+$ termination determines the number of perovskite-repeating units. We observed that, when the perovskite vertical dimension $\langle n \rangle$ is lower than a critical threshold determined by the QD diameter (~3.6 nm in this case), the perovskite layers are too thin to incorporate the QDs, resulting in a PbS QD core–perovskite shell structure. When $\langle n \rangle$ is above this threshold, QDs successfully incorporate within the perovskite flake (Fig. 1b). The resulting hybrid multidimensional QD–perovskite solid exhibits a graded-dimensionality material and energy landscape, with ensembles of layered perovskite of different repeat units where QDs are epitaxially incorporated ($CsPbBr_3$ = 5.8 Å, PbS = 5.9 Å)[23].

Ex situ grazing incidence small-angle X-ray scattering (GISAXS) studies of QDLP solid films with different QD concentrations show a dot-to-dot spacing of $q = 1.43\ nm^{-1}$ with full-width at half-maxima (FWHM) of $1.03\ nm^{-1}$ and $0.92\ nm^{-1}$ at 20–30% QD concentration (Fig. 2c,d and Supplementary Fig. 7). This confirms that the QDs are highly ordered and evenly distributed in the perovskite matrix, with an average dot-to-dot spacing of 4.4 nm. Remarkably, 2D GIWAXS shows that layered perovskites exhibit a homogeneous crystallographic orientation for 20% and 30% QD concentrations (Supplementary Figs. 8 and 10 and Supplementary Section 9).

The transient absorption (TA) spectra in Supplementary Fig. 11 show the characteristic ground-state bleaches (GSBs) of different $\langle n \rangle$ perovskites in hybrid films for different QD concentrations. These show that QDs induce a phase separation of layered perovskites, as evidenced by the evolution of the $\langle n \rangle$ distribution. In the resulting QDLP, energy transfer takes place from the larger-bandgap perovskite domains into smaller-bandgap QDs, where excitons are ultimately confined (Fig. 1a). This occurs directly or sequentially through smaller-bandgap domains.

To gain insight into the energy transfer process, we carried out photophysical spectroscopies in the QDLP system. The optical absorption spectra of bare QDLP composite films show a PbS QD exciton peak around 935 nm (Supplementary Fig. 12). Absorption features from 400 nm to 550 nm, which are characteristic of layered perovskite exciton features, are in evidence. The FWHM of the PbS QD exciton peak is ~60 nm, close to that of oleic acid (OA)-capped QDs in solution.

We then measured the PLQY of the QDLP and compared this to previous QD-in-different-perovskite systems (3D:$MAPbBrI_2$, 2D:PEA_2PbBr_4, $PEA_2Cs_2Pb_3Br_{10}$; Supplementary Fig. 13a). Photoluminescence excitation (PLE) spectra were used to further underpin energy transfer from the perovskite into the QDs (Supplementary Fig. 13b). The increase in PL intensity at excitations below the wavelength of the perovskite absorption edge is an unambiguous demonstration of efficient energy transfer from the perovskite into the QDs.

The PLQY from QDs in QDLP films (exciton peak at 935 nm) as a function of QDs concentration is shown in Supplementary Fig. 13a. Highly ordered QDLP films achieved a PLQY of 37%, similar to that of as-synthesized QDs in solution, for QD concentrations of 20–30% (QD to $PbBr_2$ mass ratio). We propose that the lack of QD aggregation maximizes exciton transfer from the matrix and minimizes self-quenching. As the QD concentration in QDLP solid films is increased beyond 20%, the PL emission from the perovskite is completely quenched, indicating efficient energy transfer from the perovskite into the QDs (Fig. 3a). This is confirmed in transient PL spectral studies (Fig. 3b), showing an evolution of carrier dynamics along with QD concentration. The PL lifetime decreases from ~13 ns for pure layered perovskite to ~1 ns for QDLPs with a 50% QD concentration.

To gain further insight into the exciton dynamics in QDLP, we tuned the pump wavelength to select between direct QD excitation and excitation primarily via the perovskite matrix (Fig. 3c,d and Supplementary Fig. 14). First, we probed QD excitons when using 675 nm excitation (wavelength longer than the perovskite band edge). The PL intensity of the QDLP films increases and redshifts as the QD concentration increases (Supplementary Fig. 14), meaning more excited near-infrared (NIR) centres emit more NIR light. Second, we excited the hybrid system using higher-energy photons of 420 nm so that excitons in the perovskite were first excited (Fig. 3c). The combination of these two excitations gives insight into energy transfer from the perovskite to the QDs. The PL peaks at different QD concentrations are at the same position regardless of the excitation wavelength (λ_{ex} = 420 nm versus λ_{ex} = 675 nm). Emission from the QDs reaches a maximum for films with a 20–30% QD concentration. We suggest that higher emission in this range can be ascribed to increased QD ordering and more oriented perovskite domains (Supplementary Figs. 7 and 8 and Supplementary Section 9). The latter can minimize unwanted exciton dissociation in the perovskite and promote efficient energy transfer[24]. PL emission decreases for higher concentrations. We attribute this to a more uneven QD landscape that leads to a different distribution of perovskite domains (which exhibits an increased presence of bulk), to a compromised QD passivation and to enhanced inter-dot interaction, in agreement

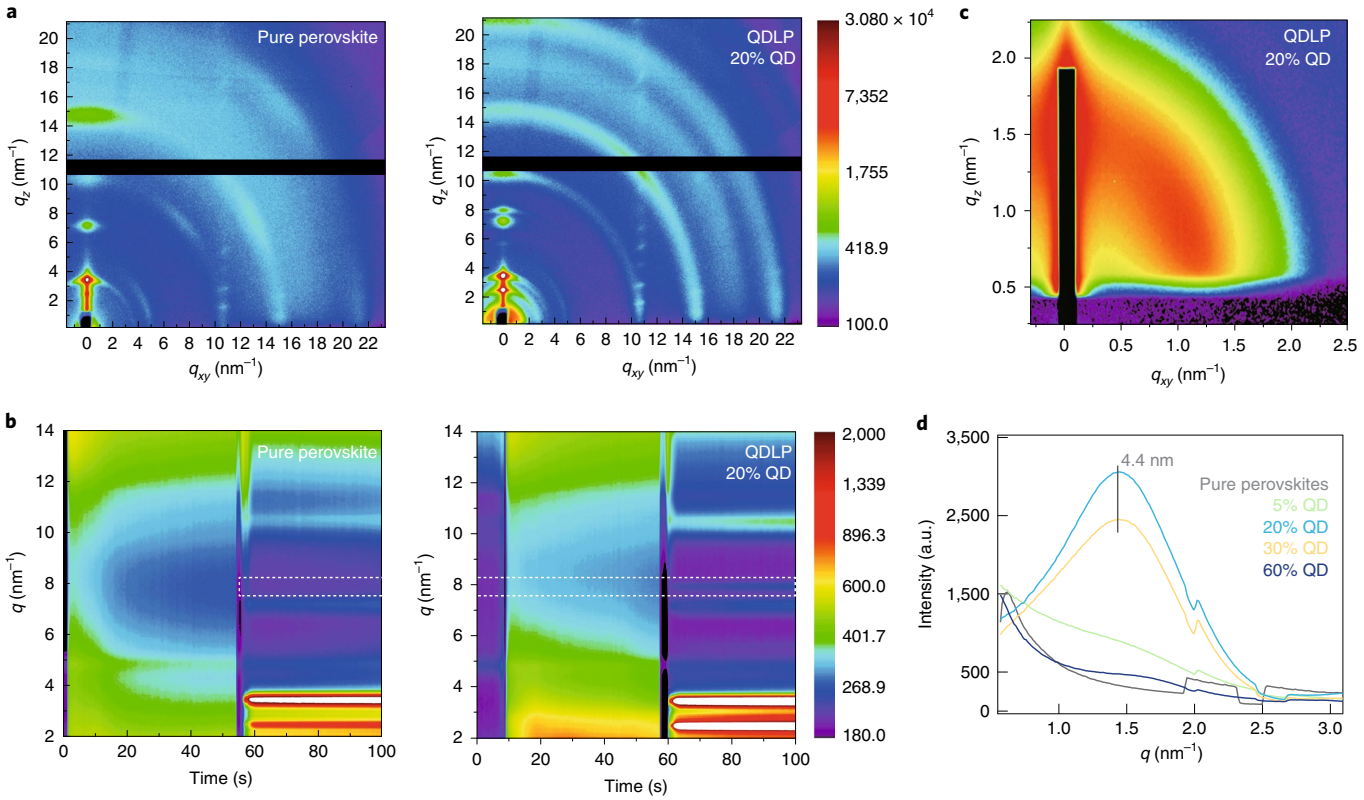

Fig. 2 | Formation kinetics of QDLP solid films. a,**b**, Ex situ (**a**) and in situ (**b**) GIWAXS of the perovskite and QDLP solid film formation process during spinning. **c**, 2D GISAXS image of QDLP solid film with 20% QD concentration. **d**, Azimuthally integrated 1D GISAXS intensities of QDLP solid film with different concentration of QDs.

with the observed larger Stokes shift (Supplementary Fig. 12). The PLE spectra of QDLP films with different concentration of QDs further confirm a more efficient energy transfer from the perovskite to the QDs in ordered systems (Supplementary Fig. 15).

To provide further insight into energy transfer in QDLP solids, we characterized the transient PL when only the QDs are excited (λ_{ex} = 723 nm) or both QDs and perovskite are excited (λ_{ex} = 374 nm) (Fig. 3d). Decay traces were fitted using a double exponential, which provided a good fit for all excitation wavelengths considered. The fast component is ascribed to surface recombination and energy transfer, while the longer decay is attributed to radiative recombination[24]. Due to the perovskite-to-QD energy transfer delay, both fast and longer decay components increase from ~90 ns to ~150 ns and from ~600 ns to ~820 ns for λ_{ex} = 723 nm and λ_{ex} = 374 nm, respectively.

To challenge the excitonic energy transfer mechanism and the impact of the QD arrangement within the QDLP solid, we fabricated carrier-selective (electron/hole only) devices (Supplementary Fig. 16). We found that devices consisting of 35% QD inclusions (highly ordered) exhibited very similar electron and hole currents. This is in contrast to other loadings, which showed larger electron currents and hence imbalanced injection. This correlates with the GISAXS, GIWAXS and photophysics experiments, which show that energy transfer was optimal when the QD arrangement was the most homogeneous.

QDLP solid films can also be tuned throughout the NIR and SWIR to emit in wavelengths spanning from 970 nm to 1,550 nm by using QDs with different sizes in different optimal arrangements of <*n*> layered perovskites[25] (Supplementary Fig. 17). The observed PLQY in the hybrid films follows that of the original as-synthesized QDs in solution (Fig. 3e). We estimated the exciton transfer efficiency from the layered perovskite to the QDs, obtaining a maximum transfer efficiency of ~82% for QDs with a 1,533 nm exciton peak (Fig. 3f and Supplementary calculation 18).

QDLPs are photostable for at least 14 h under continuous illumination in air (Supplementary Fig. 19). QDLP solids retain their initial PL intensity, in contrast with QDs in 2D or 3D perovskite matrices, for which the luminescence degrades by 10% and 40%, respectively, of the original intensity.

We then sought to take advantage of the properties of QDLP solids for LED applications. We incorporated this material as the active layer in an LED consisting of indium-doped tin oxide (ITO)/poly(3,4-ethylenedioxythiophene) poly(styrenesulfonate) (PEDOT:PSS)/QDLP layer (45 nm)/2,2′,2′′-(1,3,5-benzinetriyl)-tris(1-phenyl-1-*H*-benzimidazole) (TPBi)/lithium fluoride (LiF 10 nm)/aluminium (Al 100 nm), as shown in Fig. 4a. The corresponding band alignment of the QDLP LED device at zero bias is shown in Supplementary Fig. 20.

Based on the optimization of QD concentration and perovskite composition (Supplementary Figs. 21 and 22), QDs of different sizes were embedded into the optimal multilayered perovskite. The normalized electroluminescence (EL) of QDLP with different QD sizes shows well-defined emission peaks from the NIR to SWIR at 986, 1,097, 1,210, 1,301, 1,467 and 1,564 nm (Fig. 4b). The EQE trend as a function of QDs size follows that of PLQY × transfer efficiency (Supplementary Fig. 23). All EQE peaks are over 3%, with a highest EQE of 8.1% at 986 nm emission. For 1,310 and 1,550 nm (wavelengths of interest for fibre communication), the EQE reaches 6% and 3.5%, respectively.

To evaluate the potential of QDLP for high-brightness LED applications, we further investigated the effect of QD concentration in the active layer (Fig. 4c,d). Devices with a 35% QD content

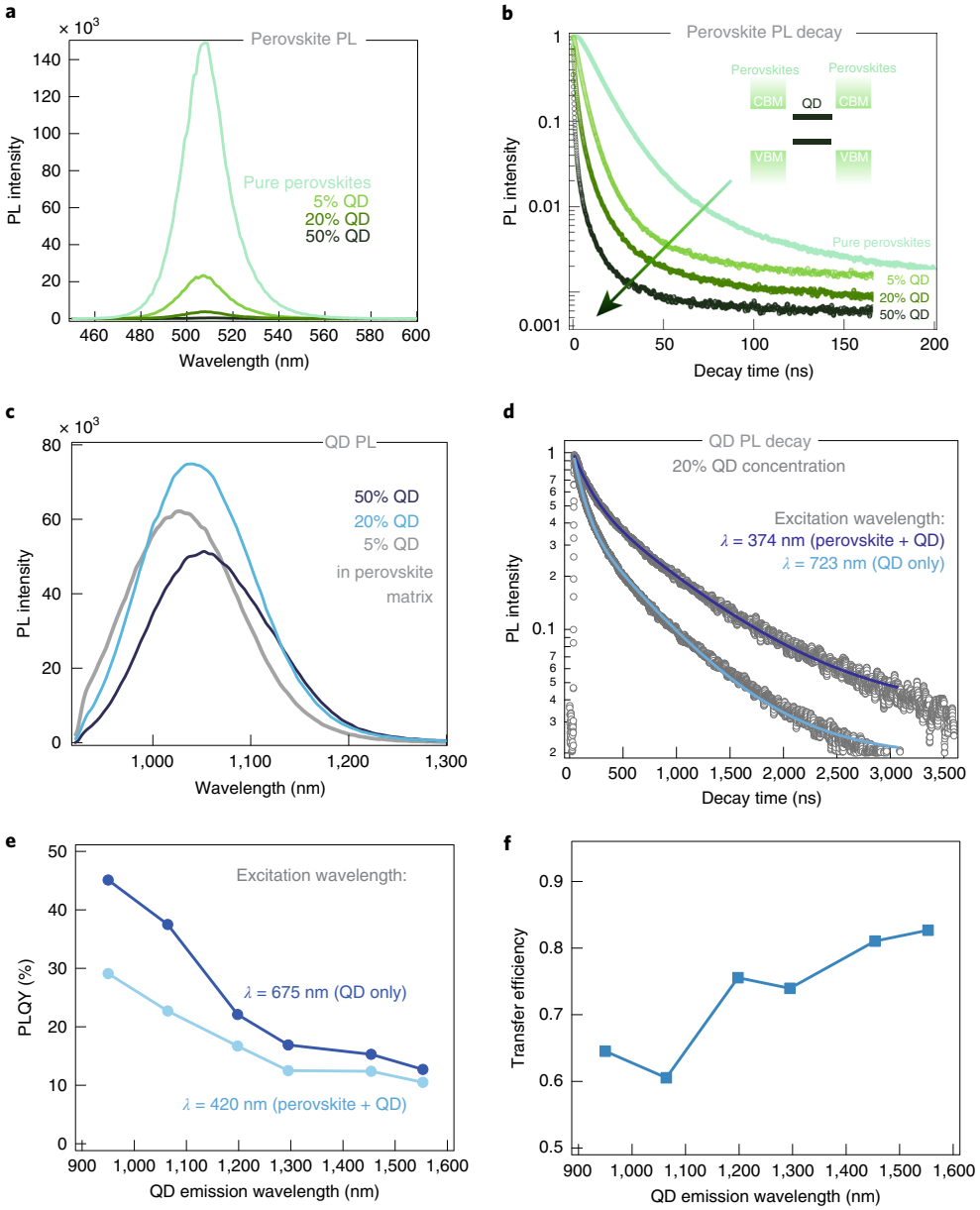

Fig. 3 | Energy transfer and PL properties of QDLP hybrid solid films. a, PL spectra of perovskite emission under 420 nm excitation (perovskites and QDs are both excited) with different concentrations of QDs. Light emission from the perovskite phase is quenched as the density of QDs in the QDLP system increases. **b**, Perovskite PL decays of QDLP films with different concentrations of QDs. **c**, PL spectra of QD emission under 420 nm excitation (perovskites and QDs are both excited). **d**, QD PL spectra of QDLP films with 20% QDs under different excitation wavelengths. **e**,**f**, PLQY (**e**) and transfer efficiency (**f**) of QDLP films with different QD sizes. The QD concentration in perovskite precursor solutions was fixed at 30%. VBM and CBM stand for valence and conduction band maximum and minimum energy levels, respectively.

can sustain an EQE of 8% up to 170 mA cm^{-2}, which then decreases due to the small carrier injection imbalance and biexciton accumulation promoting non-radiative Auger recombination. Devices with 10% and 60% QD concentration, on the other hand, show a continuous decrease in EQE as the current density increases. The 35% QD loading devices show higher EQE values and ~100 times higher J_{droop} compared to the other two samples. Optimized QDLP devices achieve a high brightness of 7.4 W Sr^{-1} m^{-2} and keep their luminance to 9 V with reduced roll-off effect. These values of EQE and the brightness of the QD LEDs operating at NIR wavelengths are high in comparison with results reported so far (for example, 5.2%[18] and 7.9%[26] EQE and 6.4 W Sr^{-1} m^{-2} radiance[1]) and we show a 40 times improvement in current when EQE droop starts to take place compared to previous PbS QD LEDs (Supplementary Table 24). EL from the perovskite phase depends strongly on QD concentration. Only when the QD concentration was below 5% did we observe EL emission from perovskites (Supplementary Fig. 25). QDLP devices show an operating stability of over 1 h at a current density of 10 mA cm^{-2} of continuous operation (Fig. 5).

QDLP devices exhibit a power conversion efficiency (PCE) peak of 1.65%, which remains above 1% up to 5 W Sr^{-1} m^{-2}. This represents a fivefold increase in PCE×brightness compared to previous QDiP LEDs[18], where the PCE drops below 1% at 1 W Sr^{-1} m^{-2} (Supplementary Fig. 26). Further improvements in PCE could be sought by reducing the large turn-on voltage in the QDLP architecture, which in the systems presented here stems from electron-/

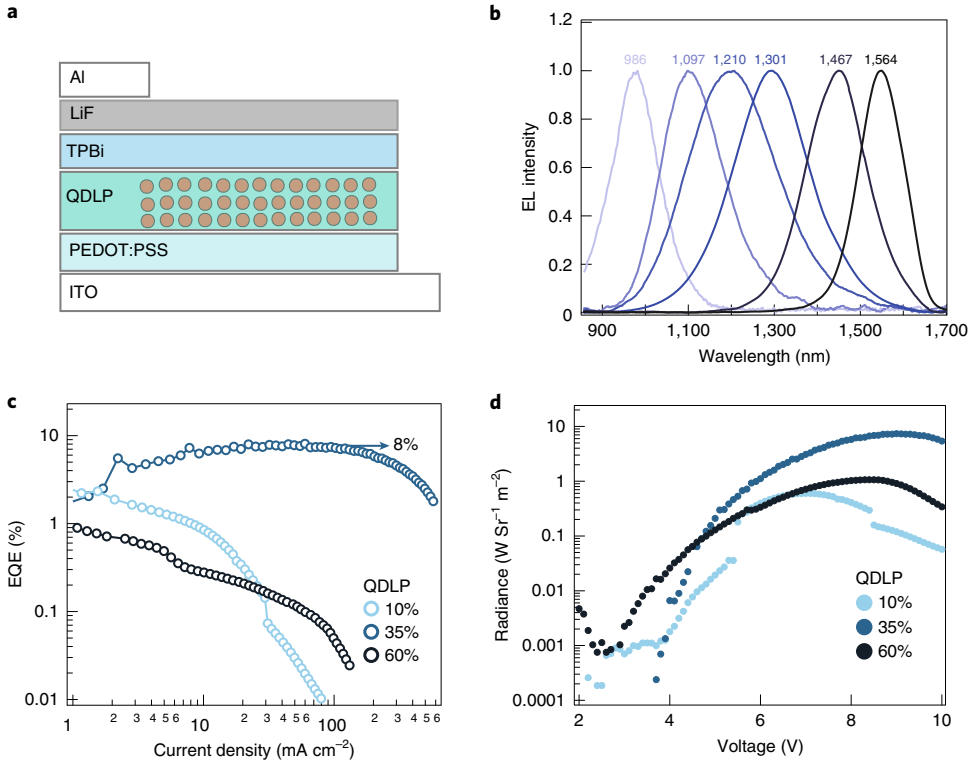

Fig. 4 | LED device performance of QDLP solids. a, LED device structure. **b**, EL spectra of QDLP solid films with different QD sizes with emission peaks spanning from 986 nm to 1,564 nm. **c**, EQE versus current density. QDLP LEDs with 35% QD inclusions, corresponding to the most homogeneous QD arrangement, sustain an EQE of 8% up to 170 mA cm^{-2}. This corresponds to a 40 times improvement in the avoidance of efficiency droop compared to QD LEDs emitting at similar wavelengths. **d**, Radiance versus voltage characteristics of QDLP LEDs with different concentrations of QDs emitting at 986 nm.

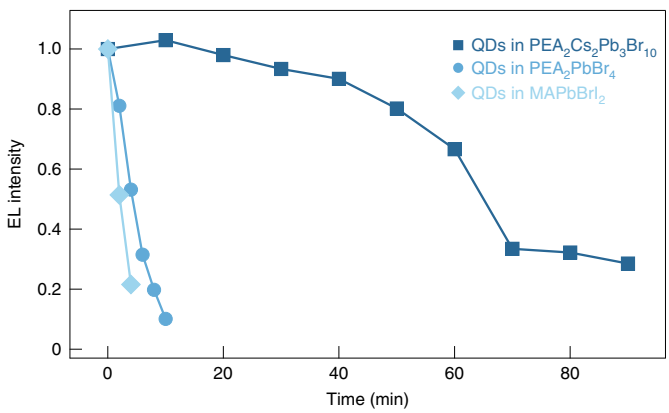

Fig. 5 | Operando stability of LEDs based on QD-in-different-perovskite films. This comparison is based on PbS QDs with a 845 nm exciton peak operating at 10 mA cm^{-2}.

hole-injecting layer (EIL/HIL) energy barriers into the large-bandgap perovskite matrix, and from the presence of PEA cations that increase device resistance. These can be pursued through the design of new perovskite matrices with lower bandgaps and less-resistive quantum wells, as well as by electrode engineering for more efficient (barrierless) injection into the matrix. Recent studies have shown promising below-bandgap turn-on voltages for QDs in matrix via density of states engineering[26–29], opening an additional promising route to the realization of bright and energy-efficient infrared LEDs.

This work demonstrates efficient infrared light-emitting materials achieved through the ordered incorporation of QDs into excitonic low-dimensional multilayered metal halide perovskites. Only when we programmed the surface of the PbS QDs to trigger a fast perovskite nucleation did we achieve QD incorporation into low-dimensional perovskite nanoplatelets, obtaining a highly ordered array of well-passivated QDs within a homogeneously oriented multilayered perovskite matrix. We tailored the dimensionality of the host perovskite system to achieve an ultrafast excitonic energy transfer into the QDs that avoids non-radiative recombination channels (for example, Auger recombination). We implemented the QDLP into LEDs that achieve a high EQE of 8.1% and a corresponding radiance of 7.4 W Sr^{-1} m^{-2} in the NIR, with a tunable emission from 986 nm to 1,564 nm. This represents a 40× improvement in the avoidance of efficiency droop compared to the best solution-processed infrared LEDs. The devices exhibit a superior operational stability compared to earlier QDiP devices, showcasing the potential of this strategy in infrared optoelectronic devices.

Online content

Any methods, additional references, Nature Research reporting summaries, source data, extended data, supplementary information, acknowledgements, peer review information; details of author contributions and competing interests; and statements of data and code availability are available at https://doi.org/10.1038/s41566-019-0577-1.

Received: 22 August 2018; Accepted: 9 December 2019;
Published online: 20 January 2020

References

1. Sun, L. et al. Bright infrared quantum-dot light-emitting diodes through inter-dot spacing control. *Nat. Nanotechnol.* **7**, 369–373 (2012).
2. Sargent, E. H. Infrared quantum dots. *Adv. Mater.* **17**, 515–522 (2005).

3. Kim, S. et al. Near-infrared fluorescent type II quantum dots for sentinel lymph node mapping. *Nat. Biotechnol.* **22**, 93–97 (2004).
4. Razeghi, M. & Nguyen, B.-M. Advances in mid-infrared detection and imaging: a key issues review. *Rep. Prog. Phys.* **77**, 082401 (2014).
5. Walther, T., Cullis, A., Norris, D. & Hopkinson, M. Nature of the Stranski–Krastanow transition during epitaxy of InGaAs on GaAs. *Phys. Rev. Lett.* **86**, 2381 (2001).
6. Yoon, J. et al. GaAs photovoltaics and optoelectronics using releasable multilayer epitaxial assemblies. *Nature* **465**, 329–333 (2010).
7. Kim, K.-H. et al. Phosphorescent dye-based supramolecules for high-efficiency organic light-emitting diodes. *Nat. Commun.* **5**, 4769 (2014).
8. Yuan, M. et al. Perovskite energy funnels for efficient light-emitting diodes. *Nat. Nanotechnol.* **11**, 872–877 (2016).
9. Wang, N. et al. Perovskite light-emitting diodes based on solution-processed self-organized multiple quantum wells. *Nat. Photon.* **10**, 699–704 (2016).
10. Xiao, Z. et al. Efficient perovskite light-emitting diodes featuring nanometre-sized crystallites. *Nat. Photon.* **11**, 108–115 (2017).
11. Shirasaki, Y., Supran, G. J., Bawendi, M. G. & Bulović, V. Emergence of colloidal quantum-dot light-emitting technologies. *Nat. Photon.* **7**, 13–23 (2013).
12. Ning, Z. et al. Quantum-dot-in-perovskite solids. *Nature* **523**, 324–328 (2015).
13. Quintero-Bermudez, R., Sabatini, R. P., Lejay, M., Voznyy, O. & Sargent, E. H. Small-band-offset perovskite shells increase Auger lifetime in quantum dot solids. *ACS Nano* **11**, 12378–12384 (2017).
14. Liu, M. et al. Hybrid organic–inorganic inks flatten the energy landscape in colloidal quantum dot solids. *Nat. Mater.* **16**, 258–263 (2017).
15. Etgar, L., Gao, P., Qin, P., Graetzel, M. & Nazeeruddin, M. K. A hybrid lead iodide perovskite and lead sulfide QD heterojunction solar cell to obtain a panchromatic response. *J. Mater. Chem. A* **2**, 11586–11590 (2014).
16. Manser, J. S. & Kamat, P. V. Band filling with free charge carriers in organometal halide perovskites. *Nat. Photon.* **8**, 737–743 (2014).
17. Chen, Z. et al. High-performance color-tunable perovskite light emitting devices through structural modulation from bulk to layered film. *Adv. Mater.* **29**, 1603157 (2017).
18. Gong, X. et al. Highly efficient quantum dot near-infrared light-emitting diodes. *Nat. Photon.* **10**, 253–257 (2016).
19. Yang, X. et al. Efficient green light-emitting diodes based on quasi-two-dimensional composition and phase engineered perovskite with surface passivation. *Nat. Commun.* **9**, 570 (2018).
20. Ng, Y. F. et al. Highly efficient Cs-based perovskite light-emitting diodes enabled by energy funnelling. *Chem. Commun.* **53**, 12004–12007 (2017).
21. Shang, Y., Li, G., Liu, W. & Ning, Z. Quasi-2D inorganic $CsPbBr_3$ perovskite for efficient and stable light-emitting diodes. *Adv. Funct. Mater.* **28**, 1801193 (2018).
22. Basheer, C. et al. Hydrazone-based ligands for micro-solid phase extraction-high performance liquid chromatographic determination of biogenic amines in orange juice. *J. Chromatogr. A* **1218**, 4332–4339 (2011).
23. Jung, Y.-K., Butler, K. T. & Walsh, A. Halide perovskite heteroepitaxy: bond formation and carrier confinement at the PbS–$CsPbBr_3$ interface. *J. Phys. Chem. C* **121**, 27351–27356 (2017).
24. Proppe, A. H. et al. Spectrally resolved ultrafast exciton transfer in mixed perovskite quantum wells. *J. Phys. Chem. Lett.* **10**, 419–426 (2019).
25. Cao, D. H., Stoumpos, C. C., Farha, O. K., Hupp, J. T. & Kanatzidis, M. G. 2D homologous perovskites as light-absorbing materials for solar cell applications. *J. Am. Chem. Soc.* **137**, 7843–7850 (2015).
26. Pradhan, S. et al. High-efficiency colloidal quantum dot infrared light-emitting diodes via engineering at the supra-nanocrystalline level. *Nat. Nanotechnol.* **14**, 72–79 (2019).
27. Pradhan, S., Dalmases, M. & Konstantatos, G. Origin of the below-bandgap turn-on voltage in light-emitting diodes and the high V_{OC} in solar cells comprising colloidal quantum dots with an engineered density of states. *J. Phys. Chem. Lett.* **10**, 3029–3034 (2019).
28. Yang, Z. et al. Mixed-quantum-dot solar cells. *Nat. Commun.* **8**, 1325 (2017).
29. Rath, A. K. et al. Remote trap passivation in colloidal quantum dot bulk nano-heterojunctions and its effect in solution-processed solar cells. *Adv. Mater.* **26**, 4741–4747 (2014).

Methods

QD synthesis and solution exchange. QDs were synthesized using previously reported methods[12]. A 3 ml volume of QDs dispersed in octane (110 mg ml^{-1}) was added into a 1 ml DMF solution containing 202 mg of PEABr. After stirring this solution vigorously for more than 6 min, QDs transferred from the top octane to the bottom DMF. The octane layer was then removed and the QDs DMF solution was washed with octane three more times to remove any organic residue. A 20 µl volume of PEA was added into the QDs DMF solution.

QDLP films and LED fabrication. $PbBr_2$ (110.1 mg) and 42.6 mg of CsBr were dissolved in 1 ml DMSO, and PEABr (202 mg) was dissolved in DMF. The desired amount of QDs in DMF containing PEABr and PEA was added into the $PbBr_2$ and CsBr DMSO solution, and the PEABr DMF solution was used to make up a 3:2:2 molar ratio of $PbBr_2$, CsBr and PEABr. The solution was spin-coated in flowing N_2 onto the substrate (at 1,000 r.p.m. for 10 s and then 3,000 r.p.m. for 60 s). Toluene was used as antisolvent, dropped after 41 s of the 3,000 r.p.m. step. The as-deposited film was annealed at 90 °C for 20 min in a N_2 glovebox to completely remove the solvent.

Pre-patterned ITO-coated glass substrates were treated with oxygen plasma for 10 min immediately before use. PEDOT:PSS purchased from Heraeus was spin-coated at 5,000 r.p.m. for 60 s in air and then annealed at 150 °C for 30 min in a N_2 glovebox. The QDLP film was spin-coated onto the PEDOT:PSS layer. TPBi (40 nm), 10 nm LiF and 100 nm Al were deposited layer by layer by thermal evaporation. Each ITO substrate was patterned to yield eight devices, each with an area of 6.14 mm^2.

Film characterization and optical property measurements. The film morphology and construction were characterized using a Scan Asyst atomic force microscope (AFM), a Hitachi scanning electron microscope, GISAXS, GIWAXS (Cornell High Energy Synchrotron Source) and an FEI transmission electron microscope. Absorption spectra were obtained using a PerkinElmer Lambda 950 system. TA measurements were conducted using an Ultrafast Helios system. PL measurements were performed using a Horiba Fluorolog system with a single grating and a time-correlated single-photon counting detector. A monochromatized Xe lamp was applied as excitation source for steady-state PL and PL excitation measurements. Pulsed laser diodes (λ_{ex} = 374 or 723 nm) were used for transient PL measurements. Standard PLQY measuments, as reported previously, were conducted in a Quanta-Phi integrating sphere coupled with optical fibres. PL stability was measured under continuous 450 nm excitation from an Xe lamp.

EL measurements and LED performance characterization. EL measurements were performed using a Keithley 2410 source meter and a NIR spectrophotometer (Ocean Optics, NIR-512) coupled with a set of lenses and optical fibre. Device stability was measured under 10 mA cm^{-2} injection in N_2 and the EL spectra were obtained continuously. *J*–*V* characteristics were monitored by a computer-controlled Keithley 2400 source meter in a N_2 atmosphere. In situ EL radiance was recorded in parallel using a calibrated Ophir PD300-IR germanium photodiode (active area of 19.6 mm^2). Lambertian emission was used to calculate the EQE and radiance according to reported standard methods. Peak EQE was calculated as the ratio of the number of emitted photons to the number of injected electrons. A minimum of 30 devices were tested for each sample type.

Data availability

Source data for Figs. 2–5 are provided with the paper. All other data that support the plots within this paper and other findings of this study are available from the corresponding authors upon reasonable request.

Acknowledgements

This publication is based in part on work supported by the Natural Sciences and Engineering Research Council of Canada, by the Ontario Research Fund Research Excellence Program, by Toyota Motors Europe and by award OSR-2017-CPF-3321-03 made by King Abdullah University of Science and Technology (KAUST). We thank R. Munir for the GIWAXS/GISAXS measurements performed at the Cornell High Energy Synchrotron Source (CHESS), supported by NSF award DMR-1332208. We thank D. Kopilovic, E. Palmiano, L. Levina and R. Wolowiec for technical support.

Author contributions

F.P.G.A. and E.H.S. designed and directed the study. L.G. and L.N.Q. led all the experimental work. Y.Z. contributed to LED device fabrication. R.M., R.Q.-B. and A.A. carried out the GIWAXS/GISAXS measurements and analysis. A.P. and L.G. carried out TA measurements. C.Z. assisted with SEM measurements. Z.Y., O.V. and J.T. helped with the design of all experimental work. All authors contributed to writing the manuscript.

Competing interests

L.G., L.N.Q., F.P.G.A., Z.Y., S.K. and E.H.S. have filed an international patent application PCT/EP2018/076830 based on the results of this manuscript.

Additional information

Supplementary information is available for this paper at https://doi.org/10.1038/s41566-019-0577-1.

Correspondence and requests for materials should be addressed to J.T. or E.H.S.

Reprints and permissions information is available at www.nature.com/reprints.